*Inorg. Chem.* **2007**, *46*, 34–43


# Speciation of the Catalytic Oxygen Evolution System: $[Mn^{III/IV}_2(\mu\text{-}O)_2(terpy)_2(H_2O)_2](NO_3)_3 + HSO_5^-$

**Hongyu Chen,[†,#] Ranitendranath Tagore,[†] Gerard Olack,[‡] John S. Vrettos,[†,§] Tsu-Chien Weng,[⊥,+] James Penner-Hahn,[⊥] Robert H. Crabtree,*[,†] and Gary W. Brudvig*[,†]**

*Departments of Chemistry and of Geology and Geophysics, Yale University, New Haven, Connecticut 06520, and Department of Chemistry, University of Michigan, Ann Arbor, Michigan 48109*

Received March 24, 2006

$[Mn^{III/IV}_2(\mu\text{-}O)_2(terpy)_2(OH_2)_2](NO_3)_3$ (**1**, where terpy = 2,2′:6′2″-terpyridine) + oxone ($2KHSO_5 \cdot KHSO_4 \cdot K_2SO_4$) provides a functional model system for the oxygen-evolving complex of photosystem II that is based on a structurally relevant Mn–$(\mu\text{-}O)_2$–Mn moiety (Limburg, J.; et al. *J. Am. Chem. Soc.* **2001**, *123*, 423–430). In this study, electron paramagnetic resonance, ultraviolet–visible spectroscopy, electrospray ionization mass spectrometry, X-ray absorption spectroscopy, and gas-phase stable isotope ratio mass spectrometry were utilized to identify the title compounds in the catalytic solution. We find that (a) $O_2$ evolution does not proceed through heterogeneous catalysis by $MnO_2$ or other decomposition products, that (b) O atoms from solvent water are incorporated into the evolved $O_2$ to a significant extent but not into oxone, that (c) the $Mn^{III/IV}_2$ title compound **1** is an active precatalyst in the catalytic cycle of $O_2$ evolution with oxone, while the $Mn^{IV/IV}_2$ oxidation state is not, and that (d) the isotope label incorporation in the evolved $O_2$, together with points a–c above, is consistent with a mechanism involving competing reactions of oxone and water with a "$Mn^V$═O" intermediate in the O–O bond-forming step.

## Introduction

In green plants and cyanobacteria, the oxygen-evolving complex (OEC) of photosystem II (PS II) catalyzes water oxidation to molecular $O_2$. Extended X-ray absorption fine structure (EXAFS) studies of PS II samples at the Mn K-edge reveal at least two 2.7-Å Mn−Mn backscattering distances that are characteristic of Mn−$(\mu\text{-}O)_2$−Mn moieties.[1−3] The recent 3.5-Å-resolution X-ray crystal structure of the PS II models the OEC as a $CaMn_3O_4$ cubane linked to a fourth Mn via a $\mu$-O bridge.[4]

EXAFS, electron paramagnetic resonance (EPR), and magnetic susceptibility studies on synthetic Mn complexes have provided important insights about the Mn tetramer in PS II. Many of those complexes, particularly the ones containing Mn−$(\mu\text{-}O)_2$−Mn moieties, have been considered as structural models for the OEC,[3,5] and yet very few complexes act as functional models.[6−9] Indeed, apart from our own system,[10−12] only three classes of metal complexes are known to catalyze homogeneous water oxidation. These

* To whom correspondence should be addressed. E-mail: gary.brudvig@yale.edu (G.W.B.), robert.crabtree@yale.edu (R.H.C.).
[†] Department of Chemistry, Yale University.
[#] Current address: Division of Chemistry and Biological Chemistry, Nanyang Technological University, Singapore 637616.
[‡] Department of Geology and Geophysics, Yale University.
[§] Current address: Human Genome Sciences Inc., Pharmaceutical Sciences, 14200 Shady Grove Road, Rockville, MD 20850.
[⊥] University of Michigan.
[+] Current address: Argonne National Laboratory, 9700 South Cass Avenue, Argonne, IL 60439.

(1) George, G. N.; Prince, R. C.; Cramer, S. P. *Science* **1989**, *243*, 789−791.
(2) Kirby, J. A.; Robertson, A. S.; Smith, J. P.; Thompson, A. C.; Cooper, S. R.; Klein, M. P. *J. Am. Chem. Soc.* **1981**, *103*, 5529−5537.
(3) Yachandra, V. K.; Sauer, K.; Klein, M. P. *Chem. Rev.* **1996**, *96*, 2927−2950.
(4) Ferreira, K. N.; Iverson, T. M.; Maghlaoui, K.; Barber, J.; Iwata, S. *Science* **2004**, *303*, 1831−1838.
(5) Manchanda, R.; Brudvig, G. W.; Crabtree, R. H. *Coord. Chem. Rev.* **1995**, *144*, 1−38.
(6) Yagi, M.; Wolf, K. V.; Baesjou, P. J.; Bernasek, S. L.; Dismukes, G. C. *Angew. Chem., Int. Ed.* **2001**, *40*, 2925−2928.
(7) Naruta, Y.; Sasayama, M.; Sasaki, T. *Angew. Chem., Int. Ed. Engl.* **1994**, *33*, 1839−1841.
(8) Gersten, S. W.; Samuels, G. J.; Meyer, T. J. *J. Am. Chem. Soc.* **1982**, *104*, 4029−4030.
(9) Ruettinger, W.; Yagi, M.; Wolf, K.; Bernasek, S.; Dismukes, G. C. *J. Am. Chem. Soc.* **2000**, *122*, 10353−10357.
(10) Limburg, J.; Brudvig, G. W.; Crabtree, R. H. *J. Am. Chem. Soc.* **1997**, *119*, 2761−2762.
(11) Limburg, J.; Vrettos, J. S.; Liable-Sands, L. M.; Rheingold, A. L.; Crabtree, R. H.; Brudvig, G. W. *Science* **1999**, *283*, 1524−1527.
(12) Limburg, J.; Vrettos, J. S.; Chen, H.; de Paula, J. C.; Crabtree, R. H.; Brudvig, G. W. *J. Am. Chem. Soc.* **2001**, *123*, 423−430.



10.1021/ic060499j CCC: $37.00 
Published on Web 12/10/2006

**Scheme 1.** Proposed Mechanism for the Catalytic $O_2$ Evolution[a,12]

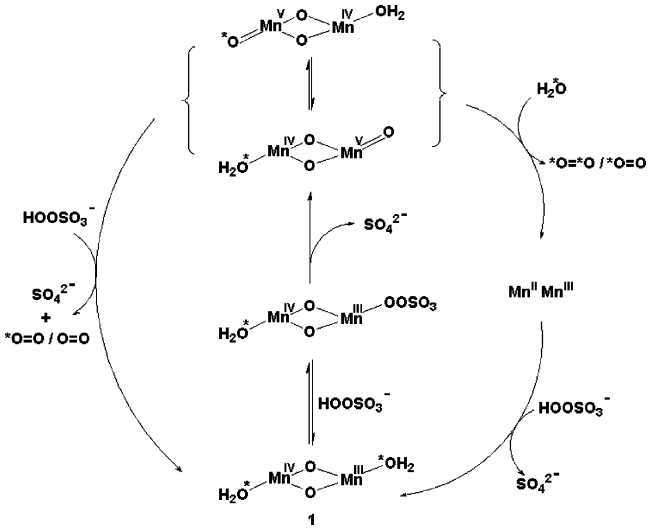


[a] O* atoms originate from water and are partially enriched with $^{18}O$ in $^{18}O$-enriched water.

involve Ru dimers,[8,13−16] Mn-bound porphyrin dimers,[7,17,18] and a carboxylate-bridged $Mn^{II/II}_2$ dimer.[19]

Our group previously reported the Mn complex $[(H_2O)(terpy)Mn^{III}(\mu\text{-}O)_2Mn^{IV}(terpy)(H_2O)]^{3+}$ (**1**), which can catalytically produce $O_2$ with >50 turnovers when oxone ($2KHSO_5{\cdot}KHSO_4{\cdot}K_2SO_4$)[10] or NaOCl[11] was used as the oxidant. When adsorbed on clay,[20] **1** has been shown to catalytically oxidize water in presence of a non-oxo-transfer oxidant, $Ce^{4+}$, as the only primary oxidant. The catalysis with oxone and NaOCl is first-order in the catalyst and follows Michaelis−Menten kinetics for the oxidants.[12] Using $^{18}O$-labeled water and unlabeled oxone, the evolved gas was collected over 1 h and analyzed using mass spectrometry. Because oxone was very slow to exchange with water,[12,21] the detection of $^{34}O_2$ and $^{36}O_2$ products clearly demonstrated the involvement of water molecules in the catalysis. In addition, a lower oxone concentration led to more $^{18}O$-label incorporation in the evolved $O_2$. A water-exchangeable $Mn^{V}{=}O$ species was proposed to undergo a competing reaction with oxone and water to give single- and double-$^{18}O$-labeled $O_2$ (Scheme 1).[12] Density functional theory calculations (B3LYP) by Siegbahn and co-workers[22] suggested that this reaction involves a $Mn^{IV}$−oxyl radical intermediate, similar to the one proposed for water oxidation in the OEC.[23,24] The barrier for O−O bond formation in this reaction was calculated to be a reasonable 23 kcal/mol.

In this report, we focus on the characterization of species involved in the catalysis using EPR spectroscopy, ultraviolet−visible (UV−vis) spectroscopy, electrospray ionization mass spectrometry (ESI-MS), X-ray absorption spectroscopy (XAS), and gas-phase stable isotope ratio mass spectrometry (SIR-MS). The real-time observation of **1** and oxone by ESI-MS during catalysis confirms the absence of O exchange between oxone and water and, in combination with the observed incorporation of O label from water into the evolved $O_2$, demonstrates the direct involvement of water in the $O_2$ evolution pathway. The rate of $O_2$ evolution correlates with the steady-state concentration of **1**, providing support for **1** being the active catalyst. Heterogeneous catalysis by $MnO_2$ is found to be insignificant.

## Experimental Section

Solutions used in the SIR-MS experiments were prepared using high-performance liquid chromatography grade water, and all other solutions were prepared using doubly deionized water. Exetainer vials used for SIR-MS experiments were purchased from Labco Inc., incubated in a pH 1 $HNO_3$ solution for 2 days, rinsed, and dried in an oven. **1**,[11] $[Mn^{IV/IV}_2O_2(terpy)_2(SO_4)_2]$ (**2**),[12] and colloidal $MnO_2$[25] were prepared following literature procedures. Oxone was purchased from Acros Organics and was standardized using iodometric titrations. Solutions of 85.5% and 95% $^{18}OH_2$ were purchased from Icon Isotopes. A stock buffer solution with ∼0.25% $^{18}OH_2$ was prepared by doping an unlabeled stock buffer solution ($[^{18}OH_2]/[OH_2]$ = 0.198 50%) with an appropriate amount of the purchased $^{18}OH_2$ solution and was standardized using SIR-MS (see the Supporting Information). All other concentrations of labeled buffer solutions were prepared by mixing the labeled stock solution with the unlabeled stock buffer. All other chemicals were purchased from Aldrich and used without further purification. Note that the label content of $^{18}O$-enriched solutions was deliberately adjusted to be only slightly above natural abundance for the SIR-MS experiments because of the extreme sensitivity of the SIR-MS instrument in the measurement of isotope ratios. This instrument is routinely used to measure very small changes in isotope ratios, which requires minimization of changes in the background isotope levels. Solutions with isotopic compositions very different from natural isotopic abundances are, therefore, incompatible with this setup.

**UV−Vis Spectroscopy.** UV−vis spectra were recorded on a Varian Cary-50 UV−visible spectrophotometer at room temperature using a 1-cm-path-length cuvette unless otherwise noted.

**EPR Spectroscopy**. Perpendicular-mode EPR spectra were collected on an X-band Varian E-9 spectrometer equipped with a $TE_{102}$ cavity and an Oxford ESR-900 liquid-helium cryostat. Parallel-mode EPR spectra were collected on a Bruker Biospin/ELEXSYS E500 spectrometer equipped with a $TE_{012}$ dual-mode cavity and an Oxford ESR-900 liquid-helium cryostat. All spectra were collected at 10 K on frozen samples with the following settings: modulation amplitude = 20 G (2 G for parallel-mode EPR spectra), modulation frequency = 100 kHz, and microwave power = 1 mW.

(13) Binstead, R. A.; Chronister, C. W.; Ni, J. F.; Hartshorn, C. M.; Meyer, T. J. *J. Am. Chem. Soc.* **2000**, *122*, 8464−8473.
(14) Geselowitz, D.; Meyer, T. J. *Inorg. Chem.* **1990**, *29*, 3894−3896.
(15) Yagi, M.; Osawa, Y.; Sukegawa, N.; Kaneko, M. *Langmuir* **1999**, *15*, 7406−7408.
(16) Sens, C.; Romero, I.; Rodriguez, M.; Llobet, A.; Parella, T.; Benet-Buchholz, J. *J. Am. Chem. Soc.* **2004**, *126*, 7798−7799.
(17) Yamamoto, K.; Nakazawa, S.; Imaoka, T. *Mol. Cryst. Liq. Cryst.* **2002**, *379*, 407−412.
(18) Shimazaki, Y.; Nagano, T.; Takesue, H.; Ye, B. H.; Tani, F.; Naruta, Y. *Angew. Chem., Int. Ed.* **2004**, *43*, 98−100.
(19) Poulsen, A. K.; Rompel, A.; McKenzie, C. J. *Angew. Chem., Int. Ed.* **2005**, *44*, 6916−6920.
(20) Yagi, M.; Narita, K. *J. Am. Chem. Soc.* **2004**, *126*, 8084−8085.
(21) Koubek, E.; Edwards, J. O.; Levey, G. *Inorg. Chem.* **1964**, *3*, 1331−1332.
(22) Lundberg, M.; Blomberg, M. R. A.; Siegbahn, P. E. M. *Inorg. Chem.* **2004**, *43*, 264−274.
(23) Siegbahn, P. E. M. *Curr. Opin. Chem. Biol.* **2002**, *6*, 227−235.
(24) Siegbahn, P. E. M. *Inorg. Chem.* **2000**, *39*, 2923−2935.
(25) Morgan, J. J.; Stumm, W. *J. Colloid Sci.* **1964**, *19*, 347−359.

**ESI-MS.** ESI-MS spectra were collected on a Waters/Micromass ZQ 4000 mass spectrometer. Owing to the weak signal at high mass, multiple scans over a narrow mass range were required to obtain a good signal/noise ratio. In all experiments involving oxone ($2KHSO_5 \cdot KHSO_4 \cdot K_2SO_4$), a KOAc/HOAc buffer was used instead of a NaOAc/HOAc buffer in order to minimize complications by ion paring. Isotope distributions were calculated using Masslynx (V4.0) and the isotope distribution calculator at http://www.siswe-b.com/mstools.htm.

**Attenuated Total Reflectance Fourier Transform Infrared Spectroscopy (ATR-FTIR)**. ATR-FTIR spectra were recorded on a Bruker Equinox FTIR spectrometer equipped with a $N_2$(l)-cooled mercury−cadmium−telluride detector. Samples were prepared by mixing a catalytic amount of **1** in water with an equal volume of oxone in water or $H_2{}^{18}O$ (95% $^{18}O$). The reaction was allowed to proceed for 3 min, and then 10 $\mu$L of the sample was dried under a stream of $N_2$ directly onto the surface of a ZnSe single-bounce internal reflection element. A total of 16 single-beam scans were collected for the sample spectrum ($R$) and a blank background ($R_0$). ATR spectra were calculated as

$$\mathrm{ATR} = -\log(R/R_0)$$

**XAS.** Mn K-edge XAS data were collected at the National Synchrotron Light Source, beamline X9-B (2.8 GeV and ∼300 mA). The XAS data were time-resolved by using a continuous-flow device. The reaction time ($t$) for a given measurement was determined by the length of the tubing from the exit end of the mixing cavity to the observation position and the flow rate of the continuous-flow apparatus.

**$^{18}$O Labeling/SIR-MS. Gas-Phase SIR-MS Instrument.** Analyses were performed using a Thermo-Finnigan GasBench II connected to a Thermo-Finnigan Delta$^{plus}$ XP stable isotope ratio mass spectrometer operating in a continuous-flow mode. Both the GasBench and Delta$^{plus}$ XP were controlled by Isodat software (version 1.5). Using the GasBench II, the headspace of a vial was sampled via a double-layered transfer needle, where He (set to 16 psi) flowed into the vial through the upper aperture (close to the septum) in the needle and the resultant mixture flowed back through the lower aperture of the same needle. The gas mixture was then directed into a Nafion (trademark of DuPont) drying tube and out through a 100-$\mu$L sampling loop in a Valco switching valve. Once the sampling loop was flushed with headspace gas, it was switched to inject the sample in the loop onto an integral gas chromatograph with a Varian CP7551 PLOT fused silica 25 m × 0.32 mm column (coating: Poraplot Q) at 32 °C to separate $O_2$ from $CO_2$. The separated gases were then carried through a second drying tube to an open split where a glass capillary would continuously draw in He and sample gases to the mass spectrometer for analysis. The dilution factor of the open split can be adjusted to decrease the signal intensity, if necessary. In the mass spectrometer, the samples were ionized (electron ionization) and analyzed in three cups set to $O_2$ peaks with masses 32, 33, and 34. The relative nominal amplifications for the three cups are 1, 100, and 300.

Under the conditions we used, the sample vials were only slightly pressurized because the sampling gas mixture from the vial either was directly vented (with the Valco valve set to "inject" mode) or was vented after going through the sampling loop (with the Valco valve set to "load" mode). A similar design has recently been reported for the study of dissolved $O_2$ in water.[26]

(26) Barth, J. A. C.; Tait, A.; Bolshaw, M. *Limnol. Oceanogr.* **2004**, *2*, 35−41.

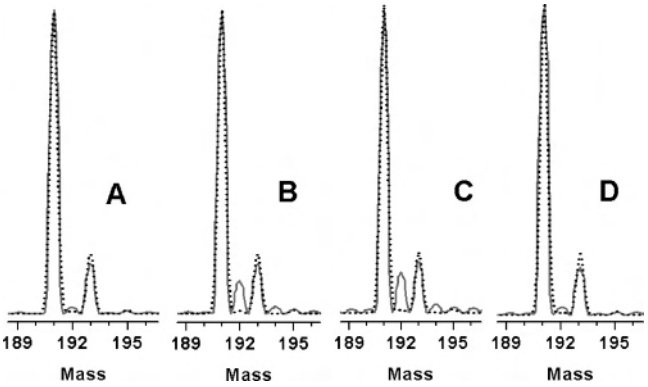


**Figure 1.** Normalized ESI-MS peaks at $m/z = 191$ ($K_2HSO_5^+$) of (A) 15 mM oxone in a 0.16 mM pH 4.5 KOAc/HOAc buffer, (B) 100 $\mu$L of solution A plus 50 $\mu$L of 85.5% $^{18}OH_2$ in $^{16}OH_2$, 2 min after mixing, (C) the same as B except 30 min after mixing, (D) 100 $\mu$L of a catalytic solution plus 50 $\mu$L of 85.5% $^{18}OH_2$ in $^{16}OH_2$, 10 min after the start of catalysis ($[\mathbf{1}]_{initial} = 1.12$ mM, [oxone] = 22.5 mM in a 0.16 mM pH 4.5 KOAc/HOAc buffer; the addition of $^{18}OH_2$ occurred within 20 s after catalysis was initialized by mixing solutions of **1** and oxone). The dotted lines are simulated spectra of $K_2HSO_5^+$. This shows that oxone does not exchange with water either in the buffer or in the catalytic solution.

**High Temperature Conversion/Elemental Analyzer (TC/EA).** Oxone samples were analyzed for bulk $^{18}O$ composition using a Thermo-Finnigan TC/EA, Conflo II, and Delta$^{plus}$ XP mass spectrometer with a Costech ZeroBlank autosampler. Approximately 200-$\mu$g samples were weighed into Ag cups, folded, sealed, then placed into the autosampler, and purged with He. Each sample, in turn, was dropped into a graphite crucible in the TC/EA furnace, a 1450 °C alumina tube with a glassy carbon tube insert filled with glassy carbon chips and a constant 90-mL/min He flow. The pyrolyzed sample released its $O_2$, which reacted with the excess C to give CO, which passed through an integral gas chromatograph (5-Å molecular sieve at 90 °C) and into the Conflo II, where ∼0.5 mL/min of the gas flow enters into the mass spectrometer for analysis. The CO produced from the samples and laboratory standards was compared to the amount in the reference CO tank in each run, and the sample values were then corrected against laboratory standards.[27,28]

## Results and Discussion

**Characterization of Species Involved in the Catalysis. (a) Oxone.** To assay O exchange between water and oxone, we monitored the peaks at $m/z = 153$ and 191 assigned to $KH_2SO_5^+$ and $K_2HSO_5^+$, respectively, in the ESI-MS spectra of an oxone solution. Incubation of oxone in a 28% $^{18}O$-labeled buffer solution for 30 min showed no significant change in the isotope peak ratio at $m/z = 153$ (not shown) and 191 (Figure 1A−C), ruling out peroxide O exchange with water at this pH and confirming the data of Koubek et al.[21] and Limburg et al.[12] More importantly, however, we now find that no such exchange occurs with water even in the presence of the Mn catalyst. Figure 1D shows the $m/z = 191$ oxone peak of a 28% $^{18}O$-labeled catalytic solution with the Mn catalyst present; again no significant changes in the isotope peak ratios were observed after 10 min. This is the same time scale as that of our catalytic reactions, where

(27) Kornexl, B. E.; Gehre, M.; Höfling, R.; Werner, R. A. *Rapid Commun. Mass Spectrom.* **1999**, *13*, 1685−1693.
(28) Vennemann, T.; Fricke, H. C.; Blake, R. E.; O'Neil, J. R.; Coleman, A. *Chem. Geol.* **2002**, 185.

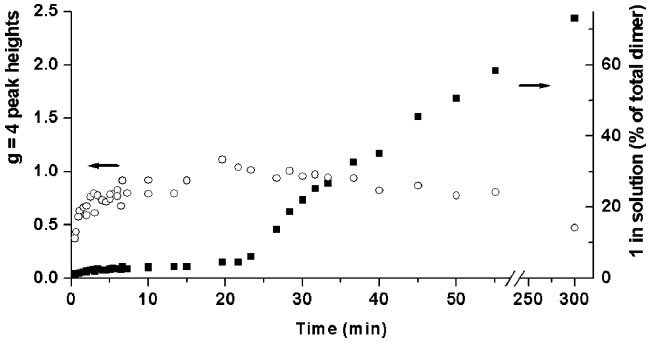


**Figure 2.** EPR measurement of the concentration change of **1** and a $g = 4$ species over the time course of catalysis. $[\mathbf{1}]_{initial} = 0.75$ mM, and $[oxone]_{initial} = 15$ mM.

oxone is usually consumed after 10−15 min. ATR-FTIR data also confirm this result (see the Supporting Information).

**(b) $[Mn^{III/IV}_2O_2(terpy)_2(OH_2)_2]^{3+}$.** To follow the speciation of Mn during catalysis, we looked in detail at the catalytic solution. ESI-MS and EPR data confirm that the $Mn_2O_2$ core of **1** is largely maintained in an acetate buffer and in the catalytic solution (see the Supporting Information). Upon the addition of an oxone solution, $Mn^{III/IV}_2$ is quickly oxidized to an EPR-silent species. While oxone was not significantly depleted in the first 10 min after mixing, the $Mn^{III/IV}_2$ concentration fell sharply to a small steady-state concentration of ∼2% of $[\mathbf{1}]_{initial}$ until oxone was depleted, after which it increased back to ∼75% of the initial value (Figure 2). ESI-MS spectra of the catalytic solutions as oxone runs out (Figure 3) show an intensity increase of peaks at $m/z = 726$ and 684 assigned to $[Mn^{III/IV}_2O_2(terpy)_2(OAc)_2]^+$ and $[Mn^{III/IV}_2O_2(terpy)_2(OAc)(OH)]^+$, respectively. The faster regeneration of the $Mn^{III/IV}_2$ peak as observed by ESI-MS, in comparison to the regeneration of the 16-line EPR signal, is probably due to faster reaction rates under the MS conditions.[29] The general correlation of the $Mn^{III/IV}_2$ peaks in ESI-MS and the intensity of the 16-line EPR signal suggests that the same $(\mu\text{-}O)_2$-bridged Mn dimer is indeed being followed by the two spectroscopic methods.

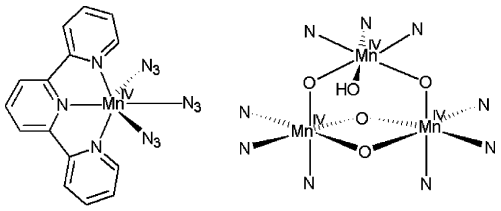

**3** **4**

**(c) $[Mn^{IV}(terpy)L_3]$ (L = $H_2O$, $HO^-$, or $AcO^-$).** Another EPR signal observed in the catalytic solution is a broad $g = 4$ signal (baseline crossover point at $g = 3.0$; Figure 4), which is not present in the initial spectrum of **1** in a NaOAc/HOAc buffer. This signal almost exactly overlaps with the EPR signal of previously identified $[Mn^{IV}(terpy)(N_3)_3]^+$ (**3**),[30] suggesting that the two species may be close in structure and coordination symmetry (Figure 4). As an alternative assignment, a $Mn^{IV}$ weakly coupled to a strongly antiferromagnetically coupled $Mn^{IV}_2O_2L_2$ dimer would also be expected to give a similar signal, as seen for $[Mn^{IV}_3O_4(OH)(bpea)_3](ClO_4)_3$ [**4**; bpea = *N*,*N*-bis(2-pyridylmethyl)ethylamine; $S = {}^3/_2$ ground state, EPR signal at $g = 4$).[31] Although the EPR signal of **4** is significantly narrower than that of **3**, presumably because of the more symmetric ligand field of the $Mn^{IV}$ ions in this complex, such a $Mn^{IV}$ trimer cannot be ruled out as the $g = 4$ species.

A $Mn^{IV/V}$ dimer (Scheme 1), another potential source of the $g = 4$ signal, could give an EPR spectrum similar to that of a $Mn^{IV}$ monomer if the $Mn^V$ $d^2$ is low-spin and electronically isolated. However, this is not supported by the stability of the $g = 4$ species in solution (Figure 4), by the absence of correlation between the $g = 4$ signal intensity and $O_2$ evolution activity, or by the XAS data, which show that the only significant valence states of Mn in solution are 3+ and 4+ (Figure 5).

**(d) Other Mn Species.** In previous work, crystals of **2** were isolated from an acidified solution of **1**[12] and crystals of $[Mn^{IV}_4O_5(terpy)_4(OH_2)_2](ClO_4)_6$ (**5**) were isolated from an acidified catalytic solution.[32] The low-pH (2.0) condition for isolation of **2** and **5** was used to facilitate the disproportionation of **1**, which gives these $Mn^{IV}$ species, but low pH may not be required for the existence of **2** and **5** in the catalytic solution. The oxidation of $Mn^{III/IV}_2$ to $Mn^{IV}$ complexes like **2** and **5** is indeed expected upon the addition of oxone because $Mn^V$ and higher oxidation states are probably too unstable. During catalysis, the presence of excess oxone keeps the concentrations of both **1** and the $g = 4$ species at low steady-state levels (Figure 2). The majority of the species in solution are EPR-silent until the depletion of oxone. When NaOCl was used as the oxidant (pH 8.6), the UV−vis absorption of the catalytic solution showed absorptions from **2** and from a substance absorbing at ∼480 nm,[11] which coincides with the absorption from **5** (470 nm in water and 480 nm in acetonitrile).[32] A 470-nm absorption was not apparent, however, in the catalytic runs at pH 4.5 using oxone as the oxidant, which rules out **5** as a significant species in the catalytic solution.

To further elucidate the proposal that **2** is dominant in the catalytic solution, we find that the ESI-MS spectrum of the catalytic solution showed about 50 peaks above the noise level between $m/z = 100$ and 1000. We found that this spectrum could be reconstructed satisfactorily from two comparison spectra: (1) a solution of 15 mM oxone in buffer and (2) a solution of 0.75 mM **2** in buffer, with 15 mM $K_2SO_4$. EPR data show that a solution of **2** in buffer contains a few percent of $Mn^{III/IV}_2$.[12] This mimics the catalytic solution, where a small percentage of Mn is in the $Mn^{III/IV}_2$ form (Figure 2), and is corroborated by the ESI-MS spectrum of **2**, which shows peaks assigned to $Mn^{III/IV}_2$ species in the catalytic solution (Figure 3), as seen in the ESI-MS spectrum

(29) Source temperature = 110 °C; desolvation gas temperature = 250 °C.

(30) Baffert, C.; Chen, H.; Crabtree, R. H.; Brudvig, G. W.; Collomb, M. N. *J. Electroanal. Chem.* **2001**, *506*, 99−105.

(31) Pal, S.; Chan, M. K.; Armstrong, W. H. *J. Am. Chem. Soc.* **1992**, *114*, 6398−6406.

(32) Chen, H.; Faller, J. W.; Crabtree, R. H.; Brudvig, G. W. *J. Am. Chem. Soc.* **2004**, *126*, 7345−7349.

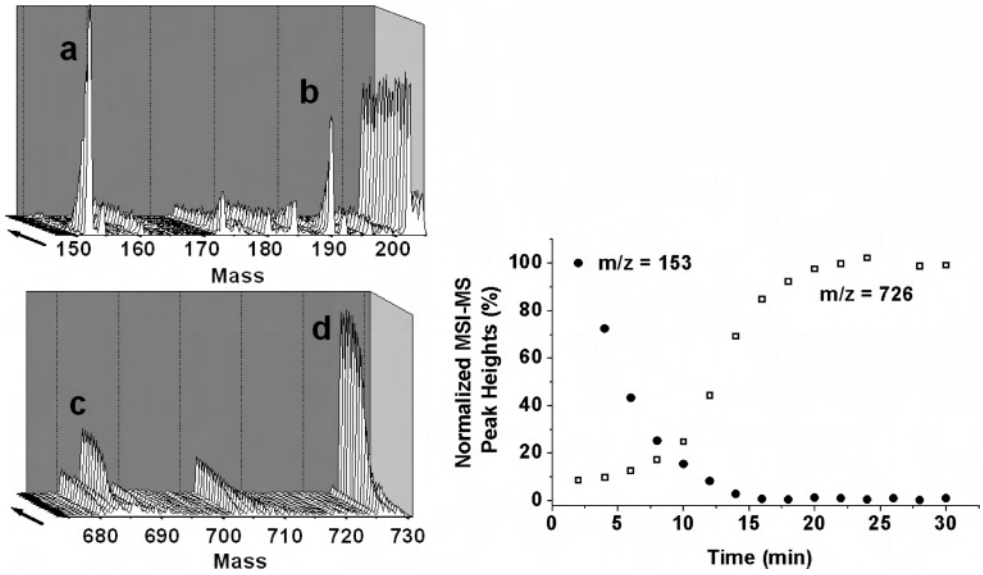


**Figure 3.** ESI-MS of the catalytic solution showing spectra of two separate runs from 2 to 30 min (arrows represent the increase of time), with 2-min intervals. Assigned peaks are (a) $m/z = 153$, $KH_2SO_5^+$, (b) $m/z = 191$, $K_2HSO_5^+$, (c) $m/z = 684$, $[Mn^{III/IV}_2O_2(terpy)_2(OAc)(OH)]^+$, and (d) $m/z = 726$, $[Mn^{III/IV}_2O_2(terpy)_2(OAc)_2]^+$. The peak between peaks c and d fits with $[Mn^{III/IV}_2O_2(terpy)_2(SO_4)]^+$ ($m/z = 704$), an expected species based on the significant concentration of sulfate in the catalytic solution. The third figure shows the peak heights of $m/z = 153$ and 726 over time.

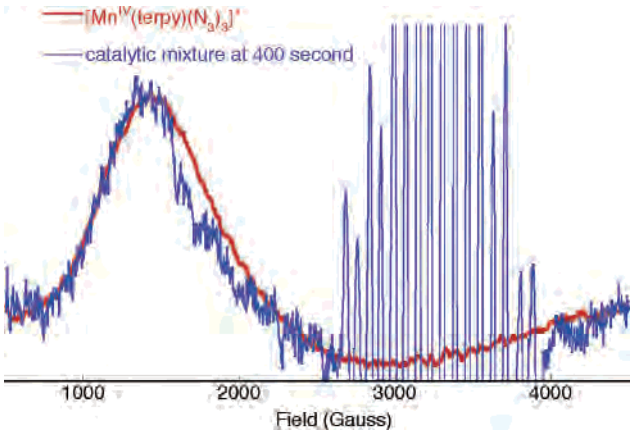


**Figure 4.** Similarity of the EPR signals, measured for frozen solutions at 10 K, of **3** and of the catalytic solution at 400 s after the start of catalysis. $[\mathbf{1}]_{initial} = 0.75$ mM, and $[oxone]_{initial} = 15$ mM.

of **2** (Figure 6). Thus, the two solutions used to simulate the spectrum of the catalytic solution give signals due to oxone, $Mn^{IV/IV}_2$, and $Mn^{III/IV}_2$ in the buffer. The two comparison spectra account for all but three peaks from the catalytic solution (Figure 6): $m/z = 202$, 265, and 287. All three are monopositive from their isotopic patterns, ruling out Mn−terpy species, which would have $m/z \geq 288$. The strongest of the three peaks, the one at $m/z = 202$, has ca. 2% of the intensity of the strongest peak in the spectrum. The inclusion of an ESI-MS spectrum of **5** under appropriate conditions as another comparison spectrum does not improve the fit to the spectrum of the catalytic solution.

These ESI-MS data provide good support for **2** being the dominant Mn species in the catalytic solution. The lack of a UV−vis peak at ~470 nm, together with the ESI-MS data, suggests that the tetramer **5** is not formed to any significant extent. Other possible forms of Mn, such as $Mn^{II}$, $Mn^{III}$, and $MnO_4^-$, were not detected (see the Supporting Information).

Further confirmation that the catalytic solution contains predominantly $Mn^{IV}$ was obtained from XAS data. The shifts in the calibrated Mn K-edge energy in the time-resolved continuous-flow XAS of the catalytic solution show that essentially all of the Mn is converted to $Mn^{IV}$ within 0.5 s after mixing oxone and **1**. At earlier times, a mixture of $Mn^{III}$ and $Mn^{IV}$ was detected (Figure 5). In summary, these results show that **1**, **2**, and a $g = 4$ species (most likely a $Mn^{IV}$ trimer or monomer) exist in the catalytic solution.

**Identification of the Active Catalyst.** Previous work has shown that the uncatalyzed decomposition of oxone is insignificant and that $O_2$ evolution is not catalyzed by $MnO_2$ or by simple Lewis acids.[10] To see if these conclusions still hold true under our conditions, we have looked at them again here.

**$O_2$ Evolution Due to Oxone Decomposition/Hydrolysis.** The spontaneous decomposition of $HSO_5^-$ was found to be fastest at the p$K_a$ (9.4) of the −O−O−H proton,[33−35] where the decomposition was proposed to involve the nucleophilic displacement of the terminal peroxidic O of $O_3SOOH^-$ by $O_3SOO^{2-}$.[21] At pH <9.4, the rate of decomposition drops linearly with the pH; extrapolation of the result of Ball and Edwards[34] gives the second-order rate constant $k_H \cong 5.4 \times 10^{-4}$ $(mol/L)^{-1}$ $min^{-1}$ at pH 4.5, slow enough to be insignificant under our conditions. SIR-MS assay of the headspace gas of a stirred oxone solution showed no $O_2$ evolution over 30 min (Figure 7), so our buffer solution contains nothing capable of catalyzing oxone decomposition.

To check for the formation of $H_2O_2$ by the hydrolysis of oxone, we injected an incubated oxone solution (1 h) into a solid $MnO_2$ powder or into a solution of **1**. SIR-MS showed

(33) Goodman, J. F.; Robson, P. *J. Chem. Soc.* **1963**, 2871−2875.
(34) Ball, D. L.; Edwards, J. O. *J. Am. Chem. Soc.* **1956**, *78*, 1125−1129.
(35) Brown, S. B.; Jones, P.; Suggett, A. *Prog. Inorg. Chem.* **1970**, *13*, 159−205.

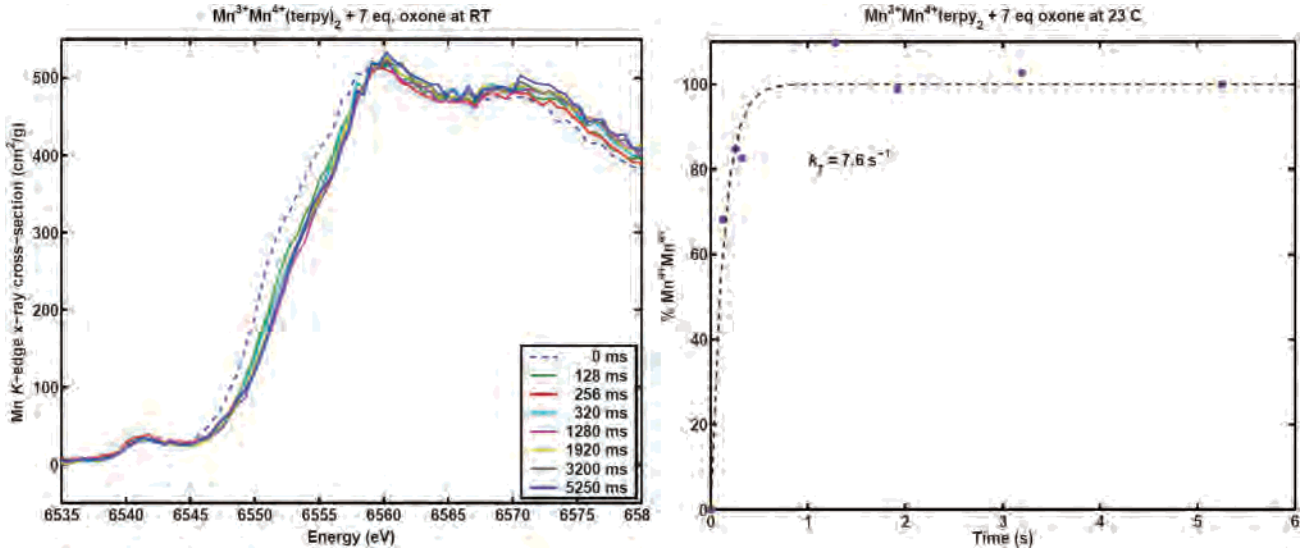


**Figure 5.** XAS data of **1** plus oxone. Left panel: Shift of the Mn K-edge upon the addition of 7 mol equiv of oxone to 1 mM **1**. The inset indicates the time after mixing for each trace. Right panel: The percentage of total Mn in the $Mn^{IV/IV}_2$ form, as determined from the edge positions in the left panel, as a function of time after mixing.

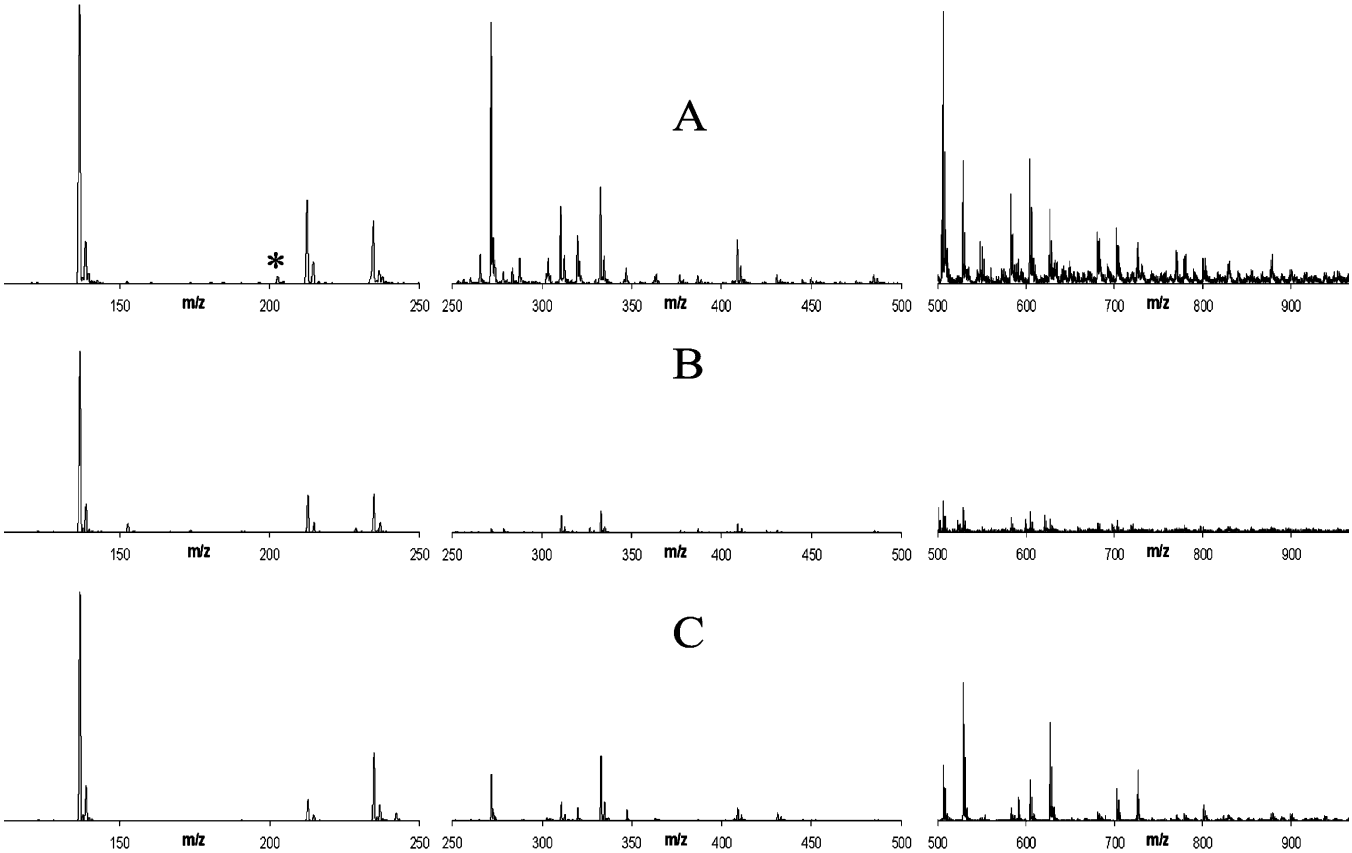


**Figure 6.** Panel A: ESI-MS spectra of the catalytic solution (0.75 mM **1** and 15 mM oxone). Panel B: ESI-MS spectra of a solution containing 15 mM oxone and 0.75 mM $KNO_3$. Panel C: ESI-MS spectra of a solution containing 0.75 mM **2**, 0.75 mM $KNO_3$, and 15 mM $K_2SO_4$. All solutions are in a 0.1 M KOAc buffer adjusted to pH4.5 with HOAc. The asterisk in panel A marks the highest intensity peak ($m/z$ = 202) in the catalytic solution that is not found in the spectrum of **2** or oxone.

no burst of $O_2$ formation, which would be expected if $H_2O_2$ were to form by hydrolysis during the incubation (Figure 7). The same activity was seen for a freshly prepared solution, so no other oxidant, such as peracid, is present. The deliberate addition of excess $H_2O_2$ instantaneously reduces a solution of **1** to a colorless state, with no further activity being seen after a burst of $O_2$ was given off that carried no $^{18}O$ label from water if the reaction was carried out in $^{18}OH_2$-labeled solutions (data not shown). This result is consistent with the observation by Dole et al. that all $O_2$ released from the oxidation of $H_2O_2$ by $MnO_2$ or $KMnO_4$ came from $H_2O_2$.[36,37] Considering the fact that catalyzed $O_2$ evolution by **1** carries the $^{18}O$ label from water (vide infra) and the observation by Dole et al. that both O atoms of $O_2$

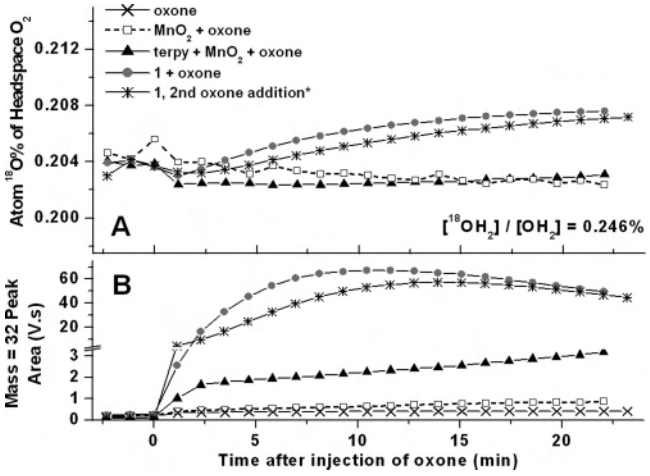


**Figure 7.** Control experiments showing the atom $^{18}O$ percentage and yield of the evolved $O_2$ against reaction time: (×) 60 mM oxone injected into an empty vial; (□) 60 mM oxone injected into a vial with 3 mg of $MnO_2$ solid; (▲) 60 mM oxone injected into the mixture of 3 mg of $MnO_2$ and 5 mg of solid terpy; (●) 15 mM oxone + 0.75 mM **1**; (*) mixture of 15 mM oxone + 0.75 mM **1** (total 4 mL) incubated for 1 h, then purged with He, and injected with 1 mL of 15 mM oxone. The increasing content of $^{18}O$ in the evolved $O_2$ with time for the catalytic solutions (● and * in part A) is due to the increasing contribution of O atoms from water relative to oxone owing to the consumption of oxone during the catalysis and the greater $^{18}O$ content of water (0.246%) relative to oxone (see below). Note that isotope ratios (top panel) derived from signal intensities (bottom panel) of less than ~1 V/s are not reliable.

evolved from $H_2O_2$ came from the peroxide, we conclude that a Mn-catalyzed hydrolysis of oxone to $H_2O_2$ and subsequent catalyzed $O_2$ evolution from $H_2O_2$ do not occur.

To test for the possibility of $O_2$ evolution via Lewis acid catalyzed hydrolysis of oxone, we previously showed that solutions of oxone with a number of Lewis acids ($Ni^{2+}$, $Zn^{2+}$, and $Al^{3+}$) gave no $O_2$ evolution.[10] We now find that $Ti^{4+}$ is similarly inactive.

**$MnO_2$-Catalyzed $O_2$ Evolution.** To eliminate the possibility that $MnO_2$ is the true catalyst, we carried out detailed studies. Solutions of **1**, especially dilute and unbuffered, are prone to decomposition to $MnO_2$ precipitate within hours. The precipitate could also be observed in the catalytic solution formed from oxone and **1** after the mixture is left for long periods (>1 h). $MnO_2$ is known to catalyze peroxide decomposition, and colloidal $MnO_2$ can catalyze heterogeneous water oxidation in the presence of manganese(IV) pyrophosphate and $Ru(bpy)_3^{2+}$,[38] so any $MnO_2$ from the decomposition of **1** might act as a catalyst for the $O_2$ evolution from oxone.

In studies to test this possibility, injection of preformed colloidal $MnO_2$ into an oxone solution leads to no $O_2$ evolution monitored by a Clark electrode. Similarly, SIR-MS experiments showed very little $O_2$ formation from the addition of an oxone solution to solid $MnO_2$ (Figure 7). The first three data sets taken before the injection of oxone are from background air (atom $^{18}O$ % = 0.204 704%); the atom $^{18}O$ percentage readings are somewhat scattered because of the low intensity of the $O_2$ peaks in the MS measurement. In the presence of terpy, however, the reaction produced more significant amounts of $O_2$, probably because of catalysis by **1** generated in situ (Figure 7). The atom $^{18}O$ percentage of headspace $O_2$ from an oxone solution containing solid terpy and $MnO_2$ stays almost unchanged and even increases slightly with time, presumably because of the dilution of background air by heavier $O_2$ evolved from water because incorporation of oxone O would drive the isotope ratio down. The fact that terpy was required for $O_2$ evolution in this case and that the evolved $O_2$ incorporates the $^{18}O$ label from solution support the proposal that a terpy-based active catalyst is formed in situ.

Previously, we reported a slower gas evolution rate upon a second addition of oxone to **1**, compared to the first addition.[12] A lower activity in the presence of degradation products argues against the latter being the true catalyst. This observation was confirmed using SIR-MS. A catalytic solution was incubated for 1 h, at which time ca. 60% of $[\mathbf{1}]_{initial}$ was regenerated (Figure 2), and then purged with He. The second addition of oxone into this solution ($[\mathbf{1}]_{initial} \approx 0.36$ mM; $[oxone]_{initial} = 12$ mM) produced significantly less $O_2$ (~35% less at $t = 7$ min) than the $O_2$ yield from the first oxone addition (Figure 7). Oxone was eventually depleted in both runs, and the balance between $O_2$ evolution and dilution by sampling He gas led to the convergence of the mass 32 peak areas.

$[Mn^{III/IV}_2O_2(bpy)_4](ClO_4)_3$ (**6**) was previously known to be unstable in an aqueous solution, and a high concentration of the bpy buffer was customarily used[39] to stabilize the complex from giving a $MnO_2$ precipitate. With excess bpy stabilizing the complex, the coordinatively saturated **6** does not catalyze $O_2$ evolution from oxone.[10] When the bpy buffer is not used, however, some $O_2$ evolution was observed (Figure 8). An initial loss of bpy is required for this reaction; the low catalytic activity of **6** could be due to either a rate-determining loss of bpy or the faster degradation of the complex. On basis of the structural similarity between **1** and **6**, it is likely that a common degradation pathway exists for the two compounds during catalysis. The less tightly binding bpy should lead to similar, if not larger, amounts of degradation products from **6**. If $MnO_2$, or any other degradation products from the catalysis, were the real catalyst for the $O_2$ evolution, **6** should not catalyze slower $O_2$ evolution than **1** under the same reaction conditions.

Because $MnO_2$ exists in many solid phases with different reactivities, it is difficult to study the reactivity of all forms with oxone. However, the following observations suggest that $MnO_2$ from the degradation of the Mn dimer cannot be the $O_2$ evolution catalyst: (a) an incubated solution (1 h) of **1** has the same activity as freshly prepared **1** (Figure 8); (b) an incubated catalytic solution has a lower activity than freshly prepared **1** (Figure 7); (c) **6** has a lower activity than **1**. Moreover, in all three of these cases, the very similar level of $^{18}O$-label incorporation from water clearly demonstrates

(36) Dole, M.; Rudd, D. P.; Muchow, G. R.; Comte, C. *J. Chem. Phys.* **1952**, *20*, 961−968.
(37) Dole, M. *Chem. Rev.* **1952**, *51*, 263−300.
(38) Shafirovich, V. Y.; Khannanov, N. K.; Shilov, A. E. *J. Inorg. Biochem.* **1981**, *15*, 113−129.
(39) Cooper, S. R.; Calvin, M. *J. Am. Chem. Soc.* **1977**, *99*, 6623−6630.

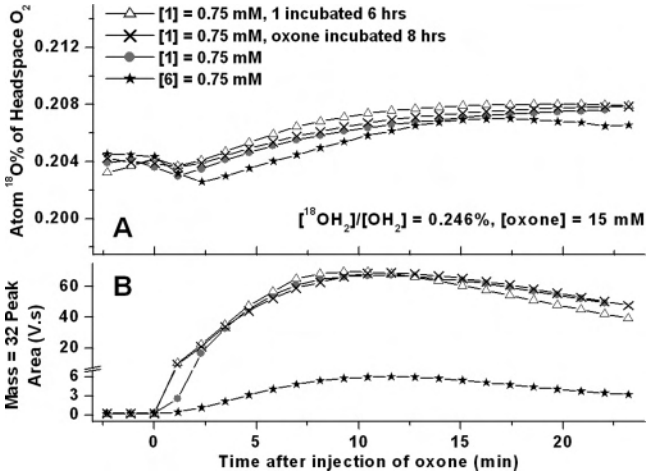


**Figure 8.** Comparison of the catalytic activities of **1** and **6**. The atom $^{18}$O percentage (A) and yield (B) of the evolved $O_2$ against the reaction time. (△) 1 mM **1** in a buffer was incubated for 6 h, into which 60 mM freshly prepared oxone solution was injected ($[\mathbf{1}]_{initial}$ = 0.75 mM; $[oxone]_{initial}$ = 15 mM). (×) $[\mathbf{1}]_{initial}$ = 0.75 mM, and $[oxone]_{initial}$ = 15 mM, with the oxone solution incubated for 8 h and the solution of **1** freshly prepared. (●) $[\mathbf{1}]_{initial}$ = 0.75 mM, and $[oxone]_{initial}$ = 15 mM, with both **1** and oxone solutions freshly prepared. (*) $[\mathbf{6}]_{initial}$ = 0.75 mM, and $[oxone]_{initial}$ = 15 mM, with both solutions freshly prepared.

that similar mechanisms are involved. The slightly lower $^{18}$O incorporation in the case of **6** could be due to a larger background air contribution to the smaller signals.

**$[Mn^{III/IV}_2O_2(terpy)_2(OH_2)_2]^{3+}$-Catalyzed $O_2$ Evolution**. Because the results in the previous section rule out degradation products as the active catalyst, the true precatalyst is, therefore, proposed to be **1**. As mentioned above, oxone oxidizes the majority of **1** to **2** at the start of catalysis, leaving low steady-state concentrations of **1** and the $g$ = 4 species. Within several minutes, both the 16-line $Mn^{III/IV}_2$ signal and the $g$ = 4 signal increase to reach a steady-state concentration. The depletion of excess oxone during catalysis is reflected by the drop of the gas evolution rate,[12] as well as by the stabilization of $^{18}$O isotope ratio readings of the headspace gas at around 20 min after the start of the reaction (Figures 9 and 10 vide infra). As oxone is depleted, the $g$ = 4 signal slowly decreases, while the $Mn^{III/IV}_2$ EPR signal starts to reappear and eventually reaches about 75% of $[\mathbf{1}]_{initial}$ (Figure 2). This correlation of **1** and oxone concentrations was clearly demonstrated by ESI-MS experiments (Figure 3c), although the reaction rates are probably faster under the MS conditions. These observations are consistent with a mechanism where **1** is the active catalyst, and the depletion of oxone leads to its regeneration.

With lower initial **1** concentrations, the catalytic $O_2$ evolution rate does not decrease linearly (parts A and B of Figure 9). In Figure 9B, the SIR-MS mass 32 peak areas at 400 s were used to estimate the relative rates of $O_2$ evolution from 0 to 400 s. Because the sampling He flow is constantly diluting the headspace gas at a constant rate, the $O_2$ loss from the dilution at any given moment is always proportional to its concentration in the headspace. The mass 32 peak area at 400 s, therefore, serves as a relative measure of the average turnover rate from 0 to 400 s. The observed saturation of the rate of $O_2$ evolution with an increase in the initial

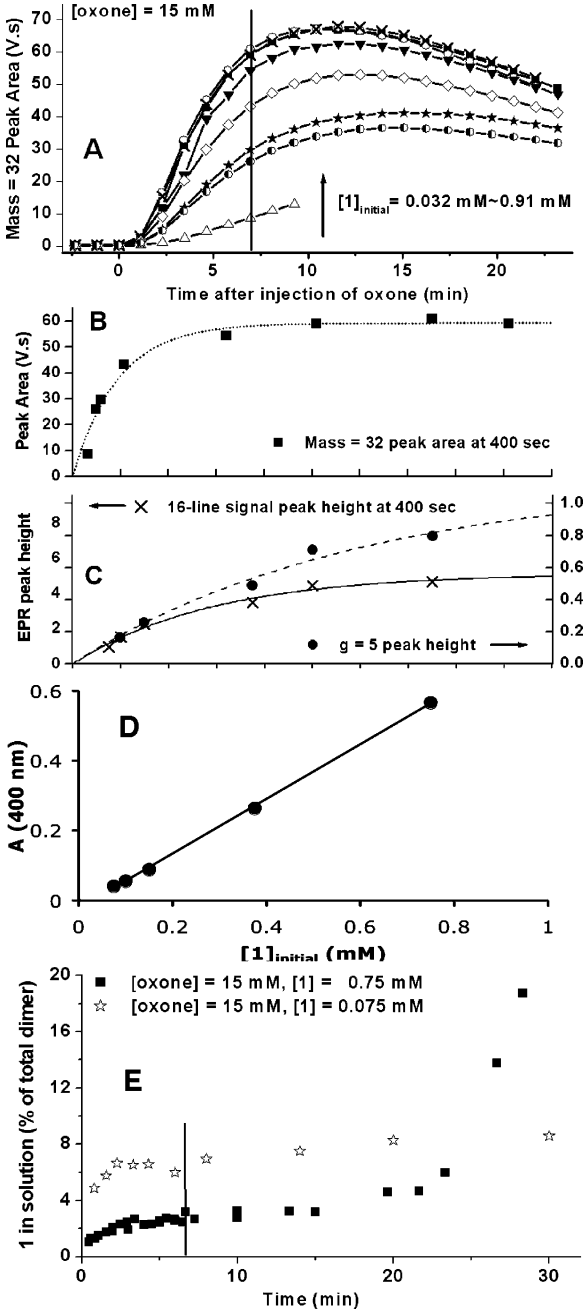


**Figure 9.** Correlation of the observed steady-state **1** EPR signal and overall $O_2$ yield at $t$ = 400 s. (A) SIR-MS peak intensity vs reaction time; $[oxone]_{initial}$ = 15 mM, and $[\mathbf{1}]_{initial}$ = 0.032, 0.048, 0.059, 0.11, 0.32, 0.51, 0.75, and 0.91 mM. The solid line marks the peaks at 400 s. (B) Peak intensity at 400 s of panel A plotted against $[\mathbf{1}]_{initial}$. (C) EPR peak heights of the catalytic solution at 400 s plotted against $[\mathbf{1}]_{initial}$ and $[oxone]_{initial}$ = 15 mM; the $g$ = 4 EPR signal intensity was measured by the amplitude of the peak at $g$ = 5. (D) 400-nm absorbance at 400 s plotted against $[\mathbf{1}]_{initial}$. (E) [**1**] in the catalytic solution, as determined by its EPR peak height with $[\mathbf{1}]_{initial}$ = 0.75 and 0.075 mM. Lines in panels B−D are guides to the eye.

concentration of **1** is not consistent with **2** being the active catalyst. While oxone is always in excess after 400 s, the EPR-silent **2** is the majority species in the catalytic solution (see above) and its concentration should be proportional to $[\mathbf{1}]_{initial}$. This is shown in Figure 9D, where the absorbance at 400 nm is taken as a measure of [**2**] in solution (see the Supporting Information) and increases linearly with $[\mathbf{1}]_{initial}$.

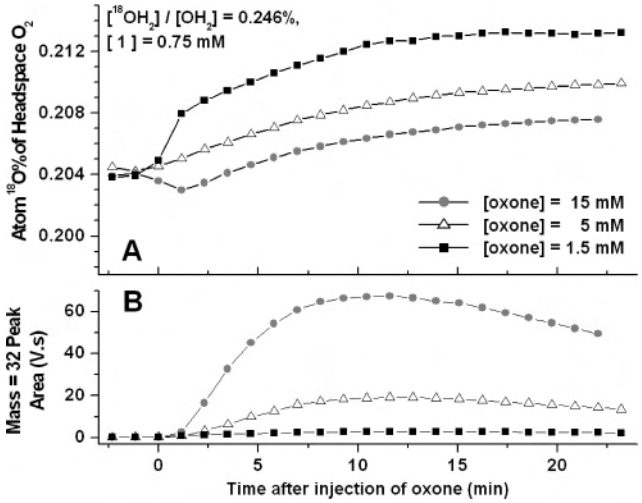


**Figure 10.** Dependence of $^{18}O$-label incorporation on $[oxone]_{initial}$. Showing the atom $^{18}O$ percentage (A) and yield (B) of the evolved $O_2$ against the reaction time.

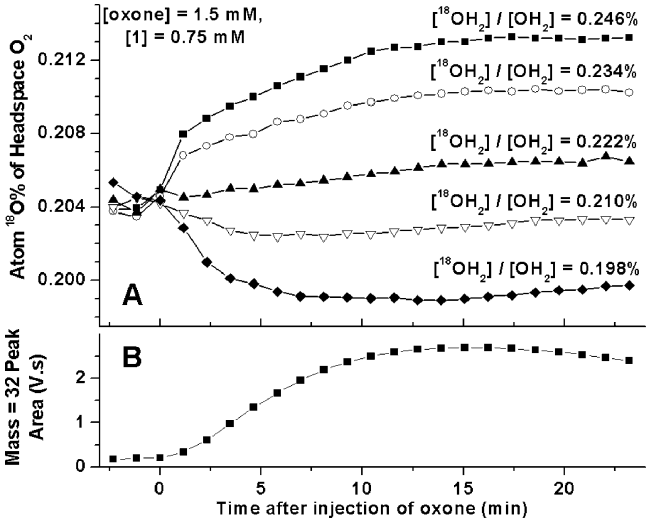


**Figure 11.** Dependence of the atom $^{18}O$ percentage of the headspace gas on the $^{18}OH_2$ concentration of the reaction mixture. The upper figure shows the atom $^{18}O$ percentage of the headspace gas vs time. The lower figure shows the mass = 32 SIR-MS peak area vs time. The first three points of each data set represent the level of residual background air. $[oxone]_{initial}$ = 1.5 mM, and $[\mathbf{1}]_{initial}$ = 0.75 mM.

If **2** were the active catalyst, the $O_2$ yield at 400 s should have been proportional to $[\mathbf{1}]_{initial}$.

Both the steady-state concentrations of **1** and the $g = 4$ species show saturation behavior with increasing $[\mathbf{1}]_{initial}$. As shown in Figure 9C, for a 5-fold drop of $[\mathbf{1}]_{initial}$ (from 0.75 to 0.15 mM), the 16-line dimer signal decreases only by 2-fold and the $g = 4$ signal decreases by 3-fold. The generally good correlation between parts B and C of Figure 9 would support a mechanism in which either of the two species is the active catalyst. Between the two candidates, the $g = 4$ species is less likely to be the active catalyst because its concentration does not correlate well with the change of the oxone concentration (Figures 2 and 3). A $Mn^{IV}$ monomer with a structure like **3** is even less likely to be the active catalyst because a $Mn^{VI}$ oxidation state is unlikely and thus makes the $Mn^{IV}$ monomer incapable of undergoing a two-electron reaction with oxone. An $S = {}^3/_2$ $Mn^{IV}$ trimer as discussed above, while unlikely to be the catalyst, cannot be completely ruled out.

On the other hand, the $Mn^{III/IV}{}_2$ concentration correlates with the rate of $O_2$ evolution, and its two-electron oxidation by oxone to form a reactive $Mn^{IV/V}{}_2$ intermediate is plausible. Because the oxidation of **1** by oxone is fast and oxone is in excess under steady-state conditions, the relative $Mn^{III/IV}{}_2$ and $Mn^{IV/IV}{}_2$ concentrations at steady state could reflect the turnover rate of the catalysis. As $[\mathbf{1}]_{initial}$ increases, most of $Mn^{III/IV}{}_2$ would be turned into the catalytically inactive **2**, the $g = 4$ species, or other EPR-silent species that do not effectively contribute to the $O_2$ evolution rate. Both parts B and C of Figure 9 show almost zero-order dependence on $[\mathbf{1}]_{initial}$ when $[\mathbf{1}]_{initial} > 0.3$ mM, strongly supporting **1** being the catalyst. At $[\mathbf{1}]_{initial} < 0.1$ mM, the $O_2$ yield of Figure 9B shows a nearly first-order dependence on $[\mathbf{1}]_{initial}$, consistent with the previously reported first-order kinetics in $[\mathbf{1}]_{initial}$ under the Clark electrode conditions ($[\mathbf{1}]_{initial}$ = 2−14 $\mu$M).[12]

**$^{18}O$-Label Incorporation from Water**. To study the involvement of water, we were able to accurately determine the isotope ratio of the evolved $O_2$ from the catalysis within 70 s by SIR-MS. This is a significant improvement over our previous setup.[12] Figure 10 shows the yield and atom $^{18}O$ percentage of the headspace $O_2$ from the catalysis in $^{18}O$-enriched solutions. In the case when $[oxone]_{initial}$ = 15 mM, the first sampling (70 s) after mixing revealed a 10-fold increase of the mass 32 peak over the background level but a decrease of the atom $^{18}O$ percentage reading. Presumably, significant incorporation of unlabeled oxone O (atom $^{18}O$ percentage estimated to be 0.2004%; see the Supporting Information) in the evolved $O_2$ diluted the heavier background air (atom $^{18}O$ % = 0.204 704%) when the concentration of oxone is high. As oxone is depleted during the catalysis, the evolved $O_2$ carries an increasingly higher level of the $^{18}O$ label; it mixes with the existing headspace $O_2$ and drives the overall atom $^{18}O$ percentage up. Within any single run, the slope of the atom $^{18}O$ percentage change between any two peaks should be determined by two factors: (a) the involvement of water O in the evolved $O_2$ during this period and (b) the dilution of this freshly evolved $O_2$ by the existing headspace $O_2$. The latter factor explains the fast initial increase of the atom $^{18}O$ percentage in the headspace but cannot account for the leveling off of the percentage because even by the second peak the background $O_2$ constitutes less than 2% of total headspace $O_2$. There have to be variations in the label incorporation from oxone and water during the catalysis. Consistent with this conclusion, decreasing the initial oxone concentration led to significantly more $^{18}O$-label incorporation into the evolved $O_2$ (Figure 10A).

The involvement of water in the catalysis is clearly demonstrated in Figure 11, in which all conditions were kept the same except the $^{18}O$ abundance of the solvent water. The use of 0:4, 1:3, 2:2, 3:1, and 4:0 mixtures of labeled ($[^{18}OH_2]$/$[OH_2]$ = 0.246 31%) and unlabeled buffer ($[^{18}OH_2]/[OH_2]$ = 0.198 50%) as the solvent led to a smooth increase in the atom $^{18}O$ percentage of the headspace $O_2$. Incorporation of

the $^{18}O$ label in the headspace gas was observed even in the first set of data collected at 70 s after the catalysis was started. Because of the complex mechanism involved, the $^{16}O/^{18}O$ isotope effects of the involved reactions cannot be fully interpreted. Theoretically, a kinetic isotope effect of 0.96 would produce significantly $^{18}O$-enriched $O_2$ ($^{18}O$ % = 0.208%) from its source ($^{18}O$ % of 0.200%; in our case, the $O_2$ sources are water and oxone). Inverse isotope effects of such magnitude were previously observed in the decomposition of $H_2O_2$[36,37] and, if occurring in our system, would need to be accounted for in the interpretation of the SIR-MS results. However, with unlabeled oxone and buffer ($^{18}O$ % of both are close to 0.200%), the final headspace $O_2$ contains 0.1997% $^{18}O$ (Figure 11). The fact that little or no fractionation of O isotopes occurred suggests that either the $^{16}O/^{18}O$ isotope effects of the catalytic reactions are insignificant or that the isotope effects of different pathways cancel out each other. In any case, the $^{16}O/^{18}O$ isotope effect should not contribute significantly to the observed $^{18}O$ abundance change in Figures 10 and 11.

The results of these $^{18}O$-labeling experiments cannot be explained by a water-exchangeable intermediate solely responsible for the label incorporation and its subsequent reaction with oxone to produce $O_2$. On this model, the dependence of $^{18}O$-label incorporation on the initial oxone concentration requires that this intermediate exchanges slower with water than it does with oxone. A lower oxone concentration could lead to an increase in the average life of this short-lived species and allow longer time for it to exchange with water (Figure 10). The initial higher concentration of oxone also limits the $^{18}O$-label incorporation, and its depletion could then allow heavier $O_2$ to be evolved. However, this mechanism would lead to only single-labeled and unlabeled $O_2$ and, therefore, is not supported by the significant yield of $^{36}O_2$ in our previous experiment.[12] Even if the postulated $Mn^V$=O intermediate had fully exchanged with $^{18}OH_2$ before reacting with oxone, the evolved $O_2$ would have contained 99.8% $^{34}O_2$ and only ca. 0.2% $^{36}O_2$. In contrast, 16 ± 8% $^{36}O_2$ was observed when $[\mathbf{1}]_{initial} = 0.75$ mM and $[oxone]_{initial} = 15$ mM.[12]

We prefer an alternative explanation in terms of a two-pathway mechanism (Scheme 1),[12] where the oxidation of steady-state **1** by oxone was proposed to generate a "$Mn^V$=O" species that can react with either oxone or water. Attack of the "$Mn^V$=O" intermediate by water will lead to some doubly labeled $O_2$, and the favoring of the oxone pathway at a high oxone concentration explains the dependence of $^{18}O$-label incorporation on the oxone concentration. For $[oxone]_{initial}$ = 1.5, 5, and 15 mM, the percent incorporation of water O in the final headspace $O_2$ ($[\mathbf{1}]_{initial} = 0.75$ mM, $t$ = 22 min; Figure 10) can be estimated to be 28%, 20%, and 16%, respectively (see the Supporting Information and Table 1). Because the proposed $Mn^V$=O intermediate has not been identified and its exchange rate with water is unknown, estimation of contributions from the two pathways is difficult. As limiting estimates, assuming a zero water exchange rate for $Mn^V$=O leads to 56%, 40%, and 32% involvement of the water pathway for $[oxone]_{initial}$ = 1.5, 5, and 15 mM, respectively. A nonzero water exchange rate of $Mn^V$=O means less involvement of the water pathway in all three cases.

## Conclusion

In this study, ESI-MS, UV−vis, XAS, and EPR spectroscopy were used to follow the real-time concentration changes of oxone and **1** in the catalytic $O_2$-evolving solution of **1** + oxone. The major species in the catalytic solution are EPR-silent $Mn^{IV}$ species as shown by XAS, mostly $Mn^{IV/IV}_2$ (**2**). A minor species exhibiting a $g = 4$ EPR signal was also observed in the catalytic solution and was assigned to be either $[Mn^{IV}(terpy)L_3]^+$ (L = $H_2O$, OH, or OAc), based on the spectral analogy with the previously identified **3**, or a 2 + 1 $Mn^{IV}$ trimer. A small amount of the mixed-valent $Mn^{III/IV}_2$ species **1** was present in the catalytic solution (<5% of total Mn) and its concentration correlated with the rate of $O_2$ evolution, suggesting a direct role in the catalysis of $O_2$ evolution. Gas-phase SIR-MS helps to precisely determine the $^{18}O$ isotope ratio of the evolved $O_2$. Incorporation of the $^{18}O$ label in $O_2$ from solution was observed, and the extent of label incorporation was found to be dependent on the oxone concentration, supporting the previously proposed competing pathway model that involves the attack of a "$Mn^V$=O" intermediate by either oxone or water. The data presented in this work provide support for the following conclusions about the mechanism of $O_2$ evolution in the present system: (a) $O_2$ evolution does not proceed through heterogeneous catalysis by $MnO_2$ or other decomposition products; (b) $O_2$ evolution does not solely occur via catalyzed decomposition of oxone; (c) the $Mn^{III/IV}_2O_2$ compound **1** is an active precatalyst in the catalytic cycle of $O_2$ evolution with oxone, while the $Mn^{IV/IV}_2$ oxidation state is not, and (d) the isotope label incorporation in the evolved $O_2$, together with points a−c above, is consistent with the mechanistic proposal in Scheme 1. Further mechanistic studies on the catalytic $O_2$-evolving system are being carried out.

**Acknowledgment.** The authors thank the National Institutes of Health (Grant GM32715) and the U.S. Department of Energy (Grant DE-FG02-84ER13297) for financial support and Christopher Incarvito for technical assistance with ESI-MS. NSF Grant CHE-0215926 for purchase of the ELEXSYS E500 EPR instrument is gratefully acknowledged. The SIR-MS studies were carried out at the Earth Systems Center for Stable Isotope Studies, a Yale Institute for Biospheric Studies research center.

**Supporting Information Available:** Details of experimental and data analysis procedures in the SIR-MS experiments, details of ATR-FTIR, EPR, and ESI-MS experiments mentioned in the text, and UV−visible spectra of **1**, **2**, and **5**. This material is available free of charge via the Internet at http://pubs.acs.org.

IC060499J